N^6-methyladenosine–Mediated Upregulation of WTAPP1 Promotes WTAP Translation and Wnt Signaling to Facilitate Pancreatic Cancer Progression

Junge Deng[1], Jialiang Zhang[1], Ying Ye[1], Kaijing Liu[1], Lingxing Zeng[1], Jingyi Huang[1], Ling Pan[1], Mei Li[2], Ruihong Bai[1], Lisha Zhuang[1], Xudong Huang[1], Guandi Wu[1], Lusheng Wei[3], Yanfen Zheng[1], Jiachun Su[1], Shaoping Zhang[1], Rufu Chen[4], Dongxin Lin[1,5,6], and Jian Zheng[1,6]

ABSTRACT

Pseudogenes may play important roles in cancer. Here, we explore the mechanism and function of a pseudogene *WTAPP1* in the progress of pancreatic ductal adenocarcinoma (PDAC). *WTAPP1* RNA was significantly elevated in PDAC and was associated with poor prognosis in patients. Overexpression of *WTAPP1* RNA promoted PDAC proliferation and invasiveness *in vitro* and *in vivo*. Mechanistically, N^6-methyladenosine (m^6A) modification stabilized *WTAPP1* RNA via CCHC-type zinc finger nucleic-acid binding protein (CNBP), resulting in increased levels of *WTAPP1* RNA in PDAC cells. Excessive *WTAPP1* RNA bound its protein-coding counterpart WT1-associated protein (WTAP) mRNA and recruited more EIF3 translation initiation complex to promote WTAP translation. Increased WTAP protein enhanced the activation of Wnt signaling and provoked the malignant phenotypes of PDAC. Decreasing *WTAPP1* RNA significantly suppressed the *in vivo* growth and metastasis of PDAC cell lines and patient-derived xenografts. These results indicate that m^6A-mediated increases in *WTAPP1* expression promote PDAC progression and thus may serve as a therapeutic target.

Significance: This study reveals how aberrant m^6A modification of the *WTAPP1* pseudogene results in increased translation of its protein-coding counterpart to promote Wnt signaling, which contributes to pancreatic cancer progression.

Introduction

Pancreatic ductal adenocarcinoma (PDAC) remains one of the deadliest malignancies with only approximately 10% of 5-year survival (1, 2). Most patients with PDAC eventually die of cancer progression due to lack of effective treatment modalities (2, 3), which poses a great medical challenge and requires urgent development of new target therapies. To achieve this, it is important to have better understanding of molecular mechanisms underlying the pathogenesis of PDAC.

Recent studies have shown that pseudogene-produced RNAs play an important regulatory role in many types of human cancer (4–6). RNAs produced by pseudogene are considered as a subclass of long ncRNAs (lncRNA) that develop from protein-coding genes but harbor multiple mutations that abrogate their translation into functional proteins (7). However, accumulating evidence has demonstrated that RNAs produced by pseudogene may function in regulating their protein-coding counterparts at either transcriptional or posttranscriptional level (5–8). While attempts have been made to explore the mechanism of anomalously expressed pseudogene RNAs in several types of cancer (5, 6, 8), little has been known about their roles and functions in PDAC.

It has been well known that RNAs are substantially modified during their maturation and aberrant modifications might cause their functional alterations and thus implicate in the development of diseases such as cancer (9–13). N^6-methyladenosine (m^6A) is the most abundant modification of RNAs that regulates RNAs at different levels such as RNA stability (9, 14–16). Recent studies have shown that some long ncRNAs are regulated by m^6A modifications and are involved in tumor progression (9, 17–21). However, there are few reports on the modifications of RNAs produced by pseudogene and their resultant roles in PDAC.

In this study, we have demonstrated a m^6A-modified RNA produced by the pseudogene *WTAPP1* as an oncogenic regulator in pancreatic cancer. We have found that CCHC-type zinc finger nucleic acid binding protein (CNBP) can recognize m^6A-modified *WTAPP1* RNA and increase its stability. Excessive *WTAPP1* RNA enhances WTAP translation through recruiting EIF3B to *WTAP* RNA. Increased WTAP level may evoke oncogenic Wnt signaling and promote PDAC progression. Furthermore, we have treated mouse models with *WTAPP1* inhibitor and the results suggest that *WTAPP1* may be a potential therapeutic target for PDAC.

[1]State Key Laboratory of Oncology in South China and Collaborative Innovation Center for Cancer Medicine, Guangzhou, Sun Yat-sen University Cancer Center, Guangzhou, China. [2]Department of Pathology, Sun Yat-sen University Cancer Center, Guangzhou, China. [3]Department of Pancreaticobiliary Surgery, Sun Yat-sen Memorial Hospital, Sun Yat-sen University, Guangzhou, China. [4]Guangdong Academy of Medical Sciences, Guangdong Provincial People's Hospital, Guangzhou, China. [5]Department of Etiology and Carcinogenesis, National Cancer Center/National Clinical Research Center/Cancer Hospital, Chinese Academy of Medical Sciences and Peking Union Medical College, Beijing, China. [6]Collaborative Innovation Center for Cancer Personalized Medicine, Nanjing Medical University, Nanjing, China.

J. Deng, J. Zhang, and Y. Ye contributed equally to this article.

Corresponding Authors: Jian Zheng, State Key Laboratory of Oncology in South China and Collaborative Innovation Center for Cancer Medicine, Guangzhou, Sun Yat-sen University Cancer Center, 651 Dongfeng Road East, 510060 Guangzhou, China. E-mail: zhengjian@sysucc.org.cn; and Dongxin Lin, E-mail: lindx@sysucc.org.cn

Cancer Res 2021;81:5268–83

doi: 10.1158/0008-5472.CAN-21-0494

Materials and Methods

Tissue specimens

Surgically removed PDAC samples and their corresponding adjacent normal tissues were collected from patients at Sun Yat-sen Memorial Hospital, Sun Yat-sen University, Guangzhou, China ($N = 158$) and Chinese Academy of Medical Sciences Cancer Hospital, Beijing, China ($N = 73$) between 2010 and 2016 (Supplementary Table S1). PDAC were confirmed histopathologically by three independent pathologists. None of the patients included in this study received any preoperative radiotherapy or chemotherapy. The patient survival time was the interval between the date of diagnosis and the date of last contact (death or last follow-up). Death information was obtained from inpatient and outpatient records or follow-up telephone calls. Written informed consent was obtained from each patient, and this study was approved by the Institutional Review Board of the Sun Yat-sen Memorial Hospital and Chinese Academy of Medical Sciences Cancer Hospital.

Pseudogene detection and differential expression analysis

We performed RNA-sequencing (RNA-seq) using 65 PDAC tumors and 33 normal tissue samples. Adaptors and low-quality bases of reads were trimmed by Cutadapt (v1.16; ref. 22), and reads shorter than 20 nucleotides were discarded. RNA-seq by expectation maximization (RSEM; ref. 23) was used to quantify gene expression. To perform a comprehensive survey of pseudogenes, we obtained the genomic information of human pseudogenes through GTF file from the GENCODE database (version 25; ref. 24) and quantified pseudogene expression as reads per kilobase per million mapped reads (RPKM). The pseudogenes with detectable expression were defined as those with an RPKM ≥ 0.1 across at least 2 samples. Finally, we identified 1,958 pseudogenes in our PDAC samples. We then used DESeq2 (25) for further differential expression analysis.

Cell lines and cell culture

Human PDAC (SW1990, Capan-2 and PANC-1) and embryonic kidney (293T) cell lines were purchased from the Cell Bank of Type Culture Collection of the Chinese Academy of Sciences, Shanghai Institute of Biochemistry and Cell Biology. All cell lines were authenticated by the DNA finger printing analysis and tested to be free of mycoplasma infection. Cells were routinely cultured in DMEM medium supplemented with 10% FBS in an atmosphere of 5% CO_2 and 99% relative humidity at 37°C.

Small interfering and guide RNAs

siRNA targeting the transcriptional products of the 10 top-candidate pseudogenes and *WTAP, METTL3, CNBP, EIF3B* genes were purchased from GenePharma (Supplementary Table S2). Transfection of siRNA (75 nmol/L) was performed with lipofectamine 2000 (Life Technologies). Two single-guide RNAs (sgRNA) adjacent to the *WTAPP1* m^{6}A site were designed (Supplementary Table S2). All guide RNAs (gRNA) were subjected to NCBI BLAST (see URLs) to avoid mismatch to unexpected RNAs in the human genome.

RNA extraction and qRT-PCR analysis

Details are provided in Supplementary Materials and Methods and the primer sequences used for qRT-PCR and other assays are shown in Supplementary Table S3.

Northern blot analysis

Approximately 50 μg of total RNA isolated from PDAC cell lines was subjected to formaldehyde gel electrophoresis and transferred to a Biodyne Nylon membrane (Pall). The RNA probes labeled with digoxigenin (Supplementary Table S4) were synthesized by Bersinbio. After prehybridization for 30 minutes, the membrane was hybridized for 12 hours at 68 °C in buffer containing the denatured probes. After washing, signal on the membrane was detected using an Odyssey infrared scanner (Li-Cor, Lincoln).

RNA immunoprecipitation assays

To determine the m^{6}A levels in *WTAPP1* RNA, total RNA from tissues or cells was extracted and subjected to fragmentation using the RNA fragmentation reagents (Ambion). Precipitation was performed using an anti-m^{6}A antibody (Synaptic Systems, 202003) previously bound to magnetic beads in RIP immunoprecipitation buffer (Magna RIP Kit, Millipore) and incubated with fragmented RNAs. After treating with proteinase K (10 mg/mL), RNAs was extracted with phenol/chloroform/isoamyl alcohol and subjected to qRT-PCR using the primers for *WTAPP1* RNA around m^{6}A site, which was normalized to input.

RNA immunoprecipitation (RIP) assays were performed using the Magna RIP RNA-Binding Protein Immunoprecipitation kit (Millipore). Antibody against CNBP, HuR, or EIF3B were used. Total RNA for each antibody were assayed simultaneously and coprecipitated RNA was detected by qRT-PCR also normalized to input.

For MS2-based RIP assays, pcDNA3.1-MS2–6X, pcDNA3.1-MS2-WTAPP1-WT, or pcDNA3.1-MS2-WTAPP1-Δ (Umine Biotechnology) was cotransfected with pMS2-GFP (Addgene) into SW1990 or Capan-2 cells with Lipofectamine 2000. RIP assays were performed using GFP antibody.

Immunoprecipitation and immunoblotting assays

PDAC cells were lysed with 1 × RIPA buffer supplemented with Protease/Phosphatase Inhibitor Cocktail (Pierce). Lysate was briefly centrifugated and the supernatant was treated with RNase A (20 μg/mL) or RNase inhibitor (200 U/mL, New England Biolab) prior to immunoprecipitation or immunoblotting with CNBP antibody. The immunoblot signal was detected using Clarity Western ECL Substrate (Thermo).

RNA pulldown and mass spectrometry analysis

RNA pulldown was performed with the Pierce Magnetic RNA-Protein Pull-Down Kit (20164, Thermo). Biotin-labeled fragment containing 50-bp *WTAPP1* RNA sequences with or without m^{6}A modification were commercially synthesized and incubated with cellular protein extracts from SW1990 and Capan-2 cells. Streptavidin beads were then added and total proteins associated was subjected to mass spectrometry (MS) or Western blot analysis. Similarly, biotinylated full-length *WTAPP1* RNA or its antisense was pulled down with the same approach and analyzed by MS or Western blotting.

RNA electrophoretic mobility shift assays

Assays were performed using the LightShift Chemiluminescent RNA EMSA Kit (Life Technologies). Biotin-labeled RNA oligonucleotides (4 nmol/L final concentration) were incubated in a 20-μL system containing binding buffer (10 mmol/L HEPES pH 7.3, 20 mmol/L KCl, 1 mmol/L MgCl2, 1 mmol/L DTT, 5% glycerol, and 40 U/mL RNasin) and various concentrations of recombinant CNBP proteins (0–10 μmol/L) at room temperature for 20 minutes. The

RNA-protein mixture was separated in 8% native polyacrylamide gels (in 0.5 × Tris-borate-EDTA buffer) at 4°C for 60 minutes. Complexes were then transferred to a nylon membrane, cross-linked to the membrane using the UVP cross-linker (120 mJ/cm^2 of 254 nm UV) and detected by chemiluminescence.

Aminomethyltrioxsalen crosslink assays

PDAC cells were suspended in PBS with or without 0.5 mg/mL of 4′-Aminomethyltrioxsalen (AMT) hydrochloride (Sigma) at a concentration of 2 × 10^7 cells/mL and incubated on ice for 15 minutes and crosslinked twice with 150 mJ/cm^2 of UV light (254 nm). Cells were pelleted for RNA isolation after cross-linking. To pull-down the *WTAP* mRNAs, 25 pmol *in vitro* transcribed and biotin-labeled *WTAPP1* RNA probes were denatured to 90°C for 2 minutes and transferred immediately on ice. Then probes and 10 μg RNA were mixed in binding buffer (50 mmol/L Tris-HCl pH 7.5, 150 mmol/L NaCl, 0.5% NP40, and 1 mmol/L ribonucleoside vanadyl complexes) and transferred to a 37°C thermomixer, shaking at 1,200 rpm for 2 hours, followed by the addition of 30 μL washed Streptavidin beads and incubated for 2 hours at room temperature. After washing, precipitated RNA was extracted by TRIzol and detected by qRT-PCR and normalized to input.

Chromatin isolation by RNA purification assays

Antisense biotin-labeled WTAP ssDNA probes were designed online (see URLs) and synthesized (Supplementary Table S4). The 13 probes were separated into 2 pools named "odd" and "even". PDAC cells (4 × 10^7) with *WTAPP1* overexpression or knockdown were used for ChIRP experiment. Cell harvesting, lysis, disruption, and ChIRP were performed as manuals of Magna ChIRP RNA Interactome Kits (Millipore). LacZ probes were used as negative probes and β-ACTIN as negative retrieved RNA and protein. *WTAP* mRNA was detected by qRT-PCR while EIF3B was detected by Western blotting.

RNA FISH and immunofluorescence

Fixed and permeabilized PDAC cells or dewaxing tumor sections were hybridized with *WTAPP1* RNA or *WTAP* RNA probes (Genepharma), or primary antibody against EIF3B or CNBP, overnight in a humidified chamber at 37°C in the dark. Cell nuclei were counterstained with DAPI. Images were taken with Olympus FV1000 confocal microscope (Olympus) for cells and with Polaris Automatic Digital Slide Scanner (Akoya Biosciences) for tissue samples.

IHC staining and scoring

Tissue microarrays purchased from Outdo Biotech Co. were IHC stained using antibody against WTAP. The IHC scoring criteria is described in Supplementary Materials and Methods.

Establishment of mouse xenograft models

Female BALB/c nude mice aged 5 weeks (Beijing Vital River Laboratory Animal Technology) were randomly grouped and injected subcutaneously with 0.1 mL of cell suspension containing 2 × 10^6 PDAC cells in the back flank. When palpable, the tumor was measured every 5 days and tumor volume was calculated by length × width^2 × 0.5. We also implanted luciferase-labeled PDAC cells (2 × 10^6) to the pancreas of mouse by surgical injection (26). Tumor volume was monitored twice a week by bioluminescence imaging with a Living Image system (Perkin Elmer) and the quantitative data were expressed as photon flux. The pancreas, lung, liver, and intestine of each mouse were removed when animal was sacrificed for further pathologic examination.

For mouse patient-derived xenograft (PDX) models, fresh PDAC samples obtained from 3 patients who underwent surgery were propagated as subcutaneous tumors in 4-week-old NOD/SCID gamma (NSG) mice (F1). Xenografts from F1 mice were cut into small pieces and then implanted into other mice (F2). When tumors grew up to about 1,500 mm^3, they were excised and cut again into small pieces and transplanted to other mice (F3; ref. 27).

Treatment of xenografts in mice

Seven days after orthotopic implantation or PDX grew up to about 200 mm^3, mice were divided into 2 groups ($n = 5$ per group) and intravenously injected with *in vivo* optimized siControl or siWTAPP1 (75 mg/kg; RiboBio; Supplementary Table S2) dissolved in saline. Treatment was performed once a day in the first 3 days and after that, once 3 days for 3 weeks (28). Tumor burden in orthotopically implantated mice was monitored twice a week by bioluminescence imaging and the PDX volume (length × width^2 × 0.5) was monitored every 3 days. The animal survival time was recorded from the day of tumor implantation to the date of death.

Animal experiments were approved by the Institutional Animal Care and Use Committee of Sun Yat-sen University Cancer Center (reference no. L102042019080W) and the animals were handled in accordance with institutional guidelines.

m^{6}A individual-nucleotide resolution cross-linking and immunoprecipitation sequencing

Total RNA from PANC-1 cells was digested with DNase I and then subjected to 2 rounds of RiboMinus (Illumina) treatment to eliminate ribosomal RNAs. The resultant RNA (200 μg) was then fragmented to about 100 nucleotides in length, incubated with 10 μg of anti-m^{6}A antibody (Synaptic Systems, 202003) before cross-linking with 150 mJ/cm^2 254-nm UV light. After incubating with Dynabeads protein A/G (Millipore) at 4°C overnight, m^{6}A-modified RNA was treated with T4 PNK (NEB) on beads, followed by proteinase K treatment, acidic phenol/chloroform extraction, and ethanol precipitation. RNA was subsequently used for library construction with NEBNext small RNA library prep kit (E7330S, NEB) and sequenced on Illumina Hiseq4000.

Identification of m^{6}A modification by iCLIP-sequencing

Read preprocessing was performed essentially as previously reported (29). Adaptors and low-quality bases were trimmed by cutadapt (v1.16; see URLs), and reads shorter than 20 nt were discarded. Reads demultiplexing based on their experimental barcode and sequence-based removal of PCR duplicates were then performed using the pyCRAC tool suite (30). The reverse reads were reversely complemented and processed in the same way as the forward counterparts. Reads were then mapped to human genome (hg38) with BWA (v0.7.15; ref. 31), with parameters "bwa aln -n 0.06 -q 20", as recommended by the online CTK Documentation (see URLs). We detected cross-linking–induced mutation sites (CIMS) and cross-linking–induced truncation sites (CITS) using CLIP Tool Kit (CTK; ref. 32). To identify the m^{6}A locus, the mode of mutation calling was performed as previously reported (33). For each mutation position, the coverages of unique tag (k) and mutations (m) were determined by CIMS.pl script of CLIP Tool Kit. We next removed the known SNPs (dbSNP 147) from all the mutation positions. Sequentially, the C > T mutation positions within m/k ≤ 50% and only mutation positions at the +1 position of adenosines were identified as CIMS-

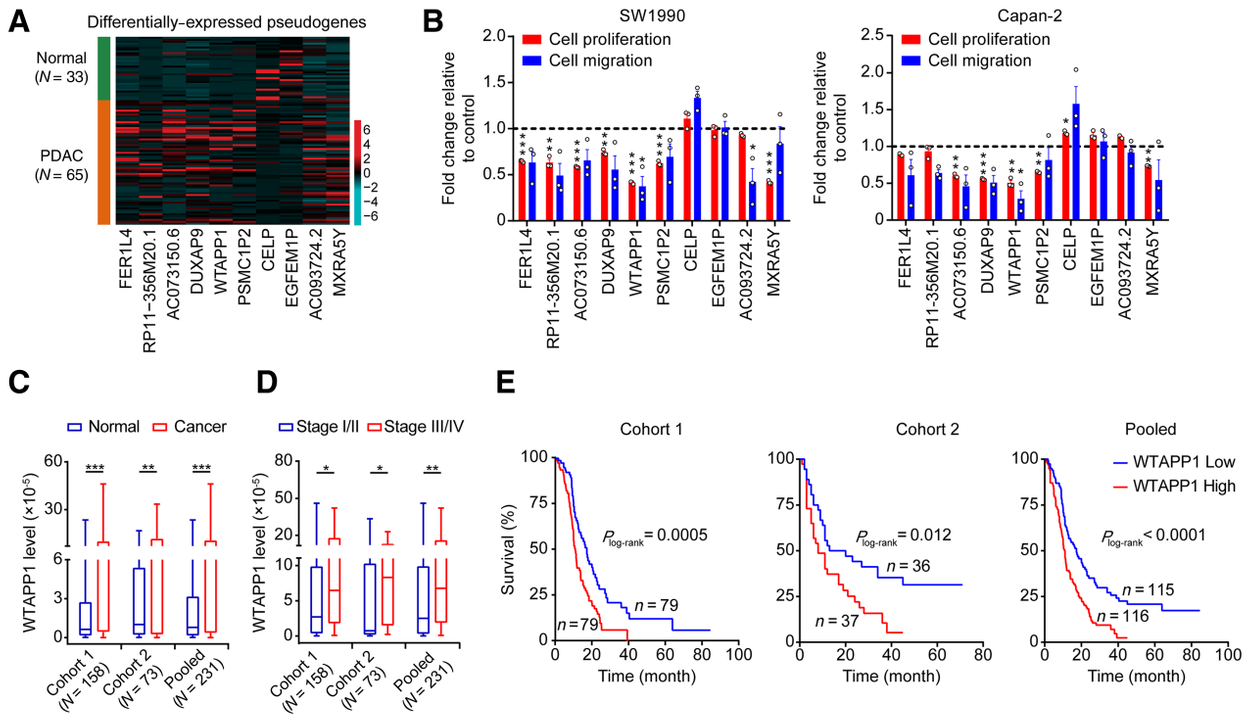

Figure 1.

WTAPP1 is overexpressed in PDAC and is associated with PDAC-cell phenotypes and clinical outcomes. **A,** Heatmap of the 10 top differentially expressed pseudogenes in 65 PDAC-tumor and 33 normal tissue samples (All FDR <0.05). Red (higher expression) or blue (lower expression) represents the normalized expression value of indicated pseudogenes. **B,** Real-time analysis of proliferation and migration of SW1990 and Capan-2 cells at time point of 96 hours (proliferation) and 18 hours (migration), which were treated with negative-control RNA or siRNA of selected 10 top differentially expressed pseudogenes. Data are mean ± SEM from three independent experiments. *, $P < 0.05$; **, $P < 0.01$; ***, $P < 0.001$ of Student *t* test. **C** and **D,** Expression levels of *WTAPP1* RNA in surgically removed PDAC samples compared with paired nontumor tissue samples (**C**) and in advanced III/IV stages compared with early I/II stages (**D**) in two cohorts and combined sample. *, $P < 0.05$; **, $P < 0.01$; ***, $P < 0.001$ of Wilcoxon rank-sum tests in **C** and Mann–Whitney tests in **D**. **E,** Kaplan–Meier estimates of survival time in two PDAC patient cohorts and combined sample by different *WTAPP1* RNA levels in tumors with HR = 1.84 [95% confidence interval (CI) = 1.29–2.64] for Cohort 1; HR = 1.89 (95% CI = 1.11–3.21) for Cohort 2; and HR = 1.88 (95% CI = 1.40–2.53) for combined sample.

based m^{6}A residues, as previously reported. Truncation sites with a significance value of $P \leq 0.05$ that occurred neighbor adenosines were retained to yield a list of CITS-based m6A residues, as online CTK Documentation recommended.

CNBP CLIP-sequencing

In brief, PANC-1 cells were washed with ice-cold PBS, cross-linked with 150 mJ/cm^2 of 254 nm UV light and harvested on ice. Cell extraction was isolated and sonicated, followed by treating with DNase I and low-dilution RNase A. Prewashed Dynabeads protein A/G conjugated with anti-CNBP antibody was incubated with the extraction at 4°C overnight with rotating. RNA was then treated with proteinase K, followed by 3′ linker ligation, acidic phenol/chloroform extraction, and ethanol precipitation. Purified RNA was reverse transcribed with Superscript III reverse transcriptase (Life Technologies) and size-selected on an 8% 1 ris-borate EDTA (TBE)–Urea gel (Life Technologies).

Identification of CNBP binding site

For the identification of CNBP-binding site, we utilized the peak calling mode of CTK with default parameters. To finally visualize each CLIP-seq dataset, we counted positional coverage across the genome by bam2wig and viewing in IGV (34).

Pancreatic cancer-cell RNA-seq and GO pathway analysis

Raw-reads processing and quantification of gene-expression level were performed as described for tissue samples. We normalized RNA-seq data as transcripts per million (TPM) for further analysis. |Foldchange| ≥ 2 (WTAPP1 knockdown versus control) were set as the cutoffs for differentially expression genes (DEG). The clusterProfiler package (35) in R was used to perform functional enrichment analysis of DEGs.

Statistical analysis

For functional analysis, results were presented as mean ± SEM of 3 or more repeated experiments. We used Student *t* test to examine the difference of mean between 2 groups. Data in abnormal distribution were analyzed by nonparametric test. Kaplan–Meier method was used to compare the survival time by different levels of *WTAPP1* RNA. Pearson correlations were calculated between *WTAPP1* RNA and their m^{6}A levels or WTAP protein levels. Correlations were considered significant and positive when $P < 0.05$ and $r > 0.30$. All statistical analyses were performed using the SPSS software package (version 20.0; IBM SPSS) and GraphPad Prism (version 8.0.0). $P < 0.05$ was considered significant for all statistical analyses.

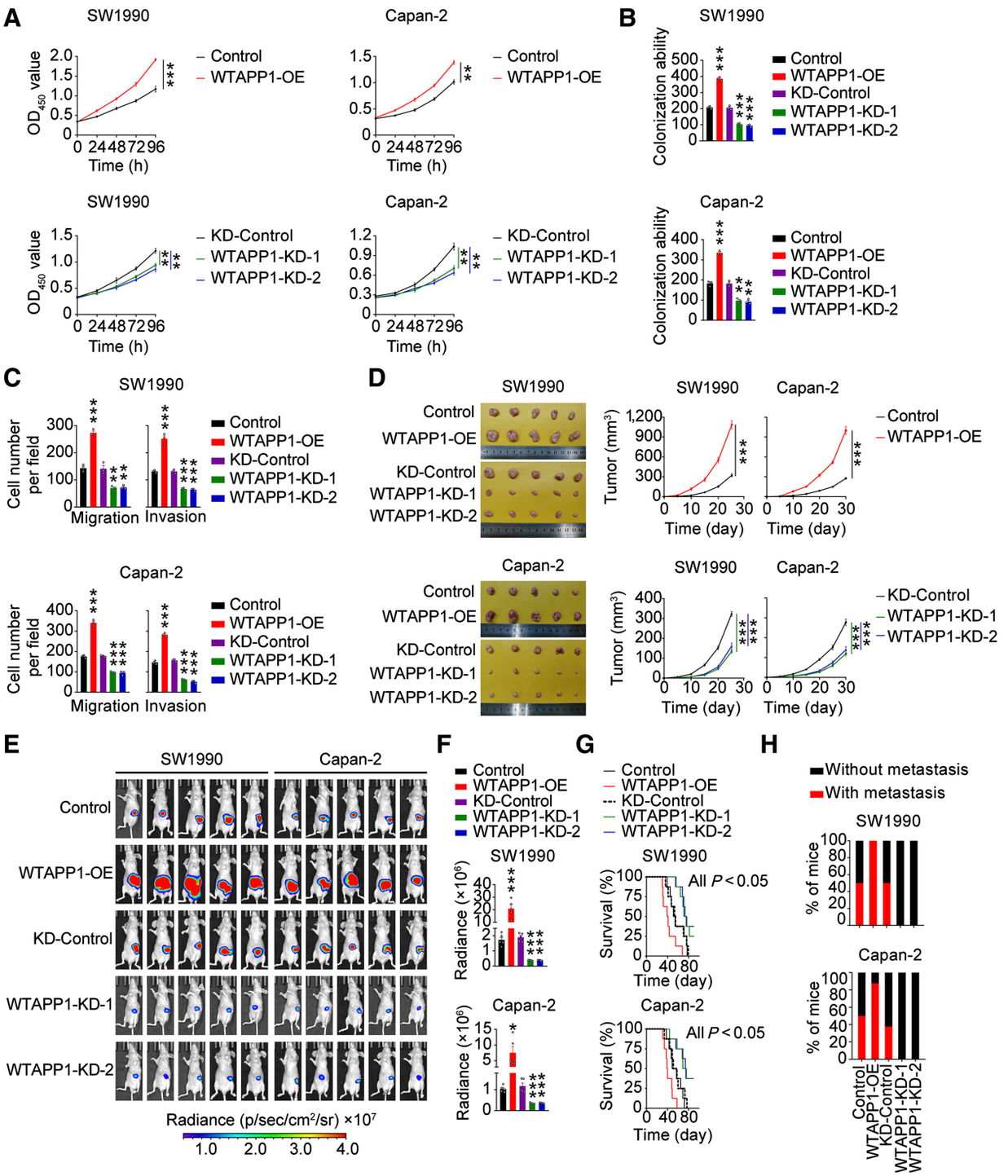

Figure 2.

WTAPP1 promotes malignant phenotypes of PDAC *in vitro* and *in vivo*. **A–C,** Effects of *WTAPP1* overexpression or knockdown on PDAC-cell proliferation (**A**), colony formation (**B**), and migration or invasion (**C**). Data are mean ± SEM from at least three independent experiments. **D,** Effects of *WTAPP1* expression change on subcutaneous PDAC xenograft growth in mice. Images of xenograft tumors (left) and tumor growth curves over time (right). Data represent mean ± SEM ($N = 5$). **E** and **F,** Effects of *WTAPP1* expression change on the growth of PDAC xenograft transplanted in mouse pancreas. Luminescence images (**E**) and quantification (**F**) of radiance intensity. Data represent mean ± SEM. **G,** Effect of *WTAPP1* expression change on survival time of mice with PDAC xenograft in the pancreas ($N = 8$). **H,** Percentage of mice with or without metastasis in each group ($N = 8$). All statistical examinations in this figure are Student *t* tests unless specified. *, $P < 0.05$; **, $P < 0.01$; ***, $P < 0.001$.

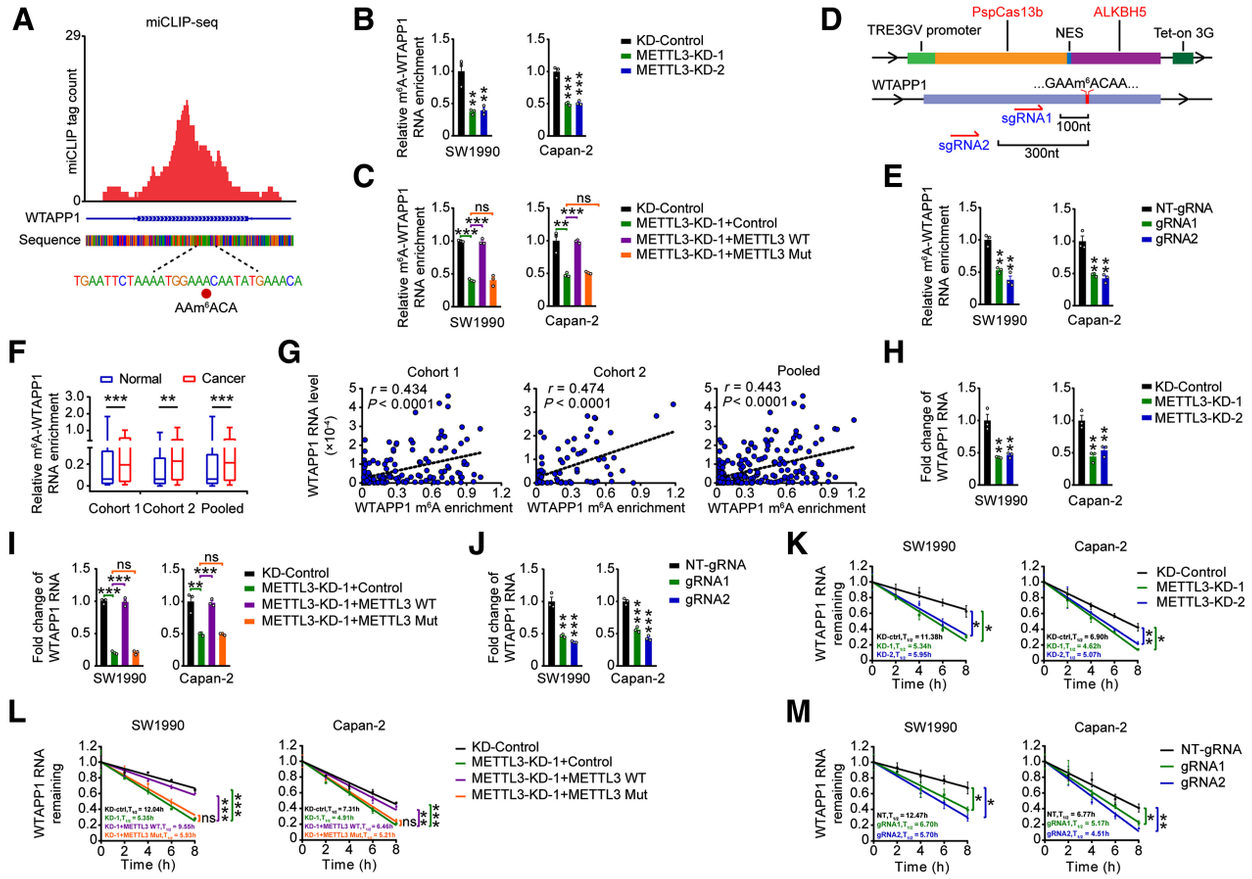

Figure 3.

m^{6}A modification increases *WTAPP1* RNA level in PDAC. **A,** Identification of m^{6}A site by miCLIP-seq in PDAC cells. The m^{6}A residue was detected by cross-linking–induced mutation site in *WTAPP1* RNA. Red tracks of miCLIP-seq are unique tag coverage and filled red circle denotes miCLIP-called m^{6}A site. **B,** Effects of *METTL3* knockdown on the levels of m^{6}A-*WTAPP1* RNA in PDAC cells. m^{6}A-*WTAPP1* RNA was detected by immunoprecipitation, followed by qRT-PCR analysis. **C,** m^{6}A-*WTAPP1* RNA levels in cells with *METTL3*-knockdown but transfected again with plasmids encoding WT *METTL3* or its catalytic mutant (aa395–398, DPPW→APPA). **D,** Schematic representation of the domain organization of dCas13b-ALKBH5 expression cassette (top) and the positions of m^{6}A site within *WTAPP1* RNA and regions targeted by two gRNAs (bottom). **E,** m^{6}A-*WTAPP1* RNA levels in PDAC cells cotransfected with doxycycline-inducible dCas13b-ALKBH5 plasmid and NT-gRNA (control) or gRNAs with doxycycline pretreatment. **F,** m^{6}A-*WTAPP1* RNA levels in PDAC compared with paired nontumor tissues in the two cohorts and combined sample. Data displayed are minimum to maximum boxplots and difference was tested by Wilcoxon rank-sum test. **G,** Correlations between *WTAPP1* RNA levels and their m^{6}A levels in PDAC tumors of patients. The correlations were analyzed by Pearson test. **H,** Effects of *METTL3* knockdown on *WTAPP1* RNA levels in PDAC cells. **I,** *WTAPP1* RNA levels in cells with *METTL3* knockdown but transfected with plasmids encoding wild-type *METTL3* or its catalytic mutant. **J,** *WTAPP1* RNA levels in PDAC cells cotransfected with doxycycline-inducible dCas13b-ALKBH5 plasmid and NT-gRNA (control) or gRNAs with doxycycline pretreatment. **K,** Half-life of *WTAPP1* RNA in cells with *METTL3* knockdown. **L,** Half-life of *WTAPP1* RNA in cells with *METTL3* knockdown but transfected with plasmids encoding WT *METTL3* or its catalytic mutant. **M,** *WTAPP1* RNA stability in PDAC cells cotransfected with doxycycline-inducible dCas13b-ALKBH5 plasmid and NT-gRNA (control) or gRNAs with doxycycline pretreatment. Student *t* tests were used to examine the difference between two means unless specifically indicated. *, $P < 0.05$; **, $P < 0.01$; ***, $P < 0.001$; ns, not significant.

Data availability

The RNA-seq data containing 65 tumor and 33 normal tissue samples in this paper have been deposited in the Genome Sequence Archive in BIG Data Center, Beijing Institute of Genomics (BIG), Chinese Academy of Sciences, under accession numbers PRCJA005425 that are publicly accessible at https://bigd.big.ac.cn/gsa. RNA-seq, m^{6}A individual-nucleotide resolution cross-linking and immunoprecipitation sequencing (miCLIP), and CNBP CLIP data have been deposited in the NCBI Short Read Archive with the BioProject ID- PRJNA693621 that are publicly accessible at https://www.ncbi.nlm.nih.gov/bioproject/?term=PRJNA693621.

For additional experimental procedures and URLs, please refer to Supplementary Materials and Methods.

Results

Identification of the pseudogene *WTAPP1* involved in PDAC

We performed RNA-seq in 65 PDAC tumor and 33 normal samples and found 104 differentially expressed pseudogenes ($\log_2$ fold change < –0.58 or $\log_2$ fold change > 0.58, FDR < 0.05; see methods) and selected 10 top pseudogenes according to the rank of their FDR values for further investigation (**Fig. 1A**). We treated 2

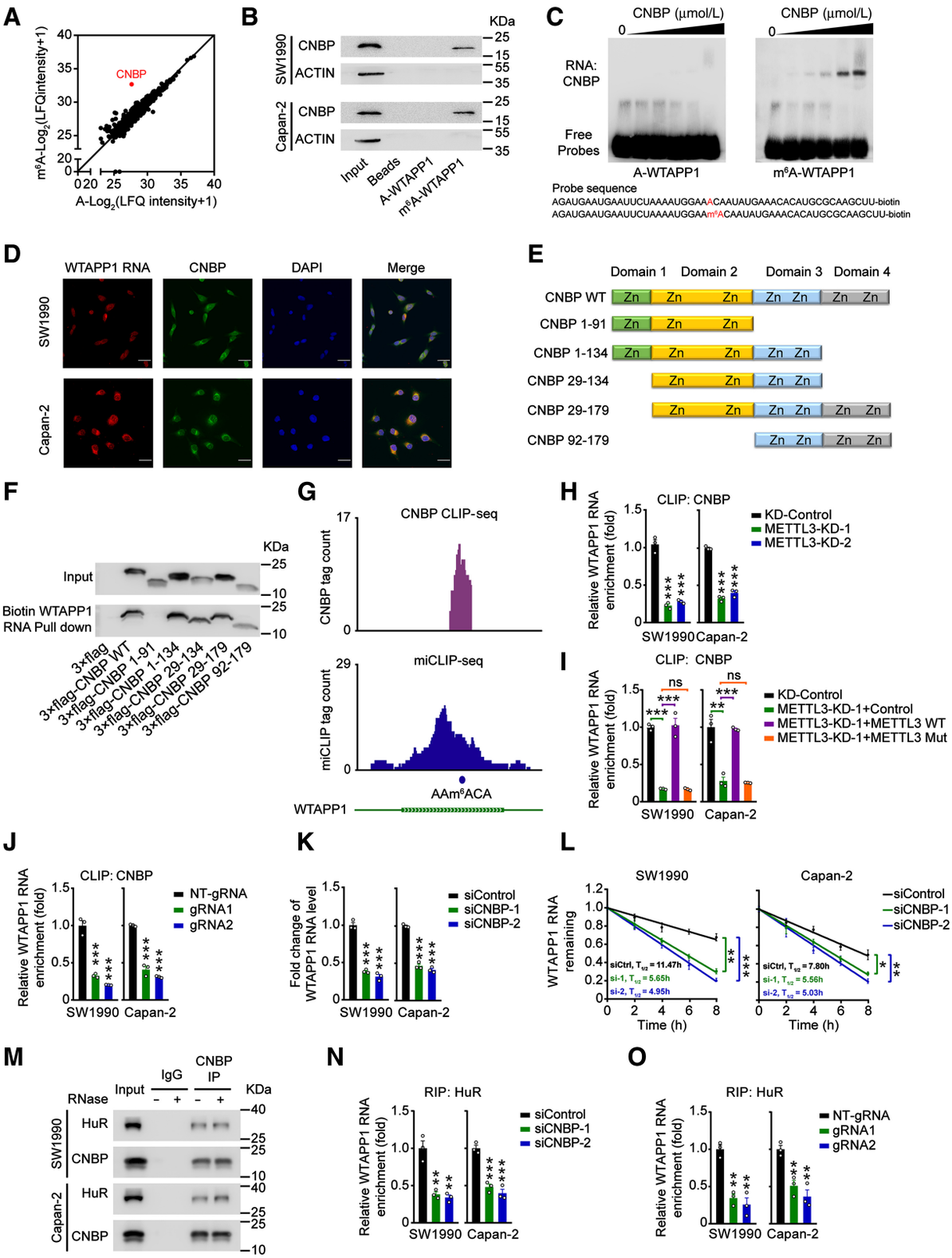
A
CNBP
m6A-Log2(LFQintensity+1)
A-Log2(LFQ intensity+1)
B
KDa
SW1990
CNBP
ACTIN
Capan-2
CNBP
ACTIN
Input
Beads
A-WTAPP1
m6A-WTAPP1
C
CNBP (μmol/L)
RNA: CNBP
Free Probes
A-WTAPP1
m6A-WTAPP1
Probe sequence
AGAUGAAUGAAUUCUAAAAUGGAAACAAUAUGAAACACAUGCGCAAGCUU-biotin
AGAUGAAUGAAUUCUAAAAUGGAAm6ACAAUAUGAAACACAUGCGCAAGCUU-biotin
D
WTAPP1 RNA
CNBP
DAPI
Merge
SW1990
Capan-2
E
Domain 1
Domain 2
Domain 3
Domain 4
CNBP WT
CNBP 1-91
CNBP 1-134
CNBP 29-134
CNBP 29-179
CNBP 92-179
Zn
F
KDa
Input
Biotin WTAPP1 RNA Pull down
3×flag
3×flag-CNBP WT
3×flag-CNBP 1-91
3×flag-CNBP 1-134
3×flag-CNBP 29-134
3×flag-CNBP 29-179
3×flag-CNBP 92-179
G
CNBP CLIP-seq
CNBP tag count
miCLIP-seq
miCLIP tag count
AAm6ACA
WTAPP1
H
CLIP: CNBP
Relative WTAPP1 RNA enrichment (fold)
KD-Control
METTL3-KD-1
METTL3-KD-2
SW1990
Capan-2
I
CLIP: CNBP
ns
KD-Control
METTL3-KD-1+Control
METTL3-KD-1+METTL3 WT
METTL3-KD-1+METTL3 Mut
J
CLIP: CNBP
NT-gRNA
gRNA1
gRNA2
K
Fold change of WTAPP1 RNA level
siControl
siCNBP-1
siCNBP-2
L
SW1990
Capan-2
WTAPP1 RNA remaining
siCtrl, T1/2 = 11.47h
si-1, T1/2 = 5.65h
si-2, T1/2 = 4.95h
siCtrl, T1/2 = 7.80h
si-1, T1/2 = 5.56h
si-2, T1/2 = 5.03h
Time (h)
M
RNase
Input
IgG
CNBP IP
KDa
HuR
CNBP
N
RIP: HuR
O
RIP: HuR

frequently used PDAC cell lines, SW1990 and Capan-2, with siRNAs targeting these 10 pseudogenes and the resultant cell proliferation and migration changes were monitored with xCELLigence technology. The results suggested that, only siWTAPP1 was able to suppress cell proliferation and migration in both cell lines (**Fig. 1B**). We then examined the *WTAPP1* RNA levels in Cohort 1 ($N = 158$) and Cohort 2 ($N = 73$) patients with PDAC (Supplementary Table S1) and the results showed that the levels of *WTAPP1* RNA were significantly higher in tumors than in adjacent normal tissues (**Fig. 1C**) and in stages III/IV PDACs than in stages I/II PDACs (**Fig. 1D**). Kaplan–Meier analysis showed that PDAC patients with high *WTAPP1* RNA level (≥ median) had worse prognosis and shorter overall survival time than those with low *WTAPP1* level (< median; **Fig. 1E**). We also analyzed The Cancer Genome Atlas (TCGA) data and the Genotype-Tissue Expression (GTEx) data from the GEPIA online database (see URLs) and also found that the *WTAPP1* RNA levels were significantly upregulated in PDAC (Supplementary Fig. S1A) and high levels were correlated with short overall survival time (Supplementary Fig. S1B).

We then performed experiments to characterize *WTAPP1* RNA in PDAC cell lines and found that it presents at about 100 copies per cell and dominantly located in the cytoplasm (Supplementary Fig. S1C–S1E). Coding potential calculator based on sequence intrinsic features (CPC, see URLs) identified *WTAPP1* as a noncoding transcript (Supplementary Table S5). UniProt human-protein profile of 20 PDAC cell lines in Cancer Cell Line Encyclopedia (CCLE) identified no peptides matching *WTAPP1* ORFs (Supplementary Fig. S1F, Supplementary Table S5). Experimentally, FLAG-fused tagging of putative protein assays confirmed that the WTAPP1–FLAG fusion proteins did not exhibit the predicted relative molecular weight determined by Western blotting. The assays included MYC (FLAG-tagged) as a positive control and lncRNA without coding potential, WSPAR (FLAG-tagged), as a negative control (Supplementary Fig. S1G; ref. 36). Furthermore, ribosome sedimentation analysis revealed that similar to classic noncoding RNA *XIST*, *WTAPP1* RNA has low affinity for polysome (Supplementary Fig. S1H), suggesting that it may not have protein-producing ability and is a *bona fide* pseudogene involved in PDAC prognosis.

WTAPP1 RNA promotes PDAC cells proliferation and invasiveness

We then investigated the role of *WTAPP1* RNA by changing its expression in PDAC cell lines (Supplementary Fig. S2A). Overexpressing *WTAPP1* substantially enhanced the abilities of PDAC-cell proliferation, colony formation, migration, and invasion *in vitro*, while silencing *WTAPP1* had opposite effects (**Fig. 2A–C** and Supplementary Fig. S2B and S2C). These effects were further verified *in vivo* in mouse xenograft models. Subcutaneous xenografts derived from PDAC cells overexpressing *WTAPP1* had significantly increased growth rates while tumors derived from *WTAPP1* silencing PDAC cells had significantly reduced growth rates compared with each control (**Fig. 2D**). We also implanted PDAC cells in mice pancreas and tested the effect of *WTAPP1* on tumor metastasis. The results showed that *WTAPP1* overexpression significantly increased distant metastasis of PDAC cells and reduced animal survival time, while *WTAPP1* silence had opposite effects (**Fig. 2E–H**; and Supplementary Fig. S2D, Supplementary Table S6). Taken together, these results indicate that *WTAPP1* is an oncogenic pseudogene capable of promoting proliferation and metastasis of PDAC cells.

m^{6}A modification of *WTAPP1* RNA and the consequences

To explore why *WTAPP1* is overexpressed in PDAC, we analyzed genomic alterations including mutations and CNAs of *WTAPP1* in PDAC tissues derived from different datasets and the results were negative (Supplementary Fig. S3A). We did not find any CpG islands in the promoter region of *WTAPP1* and the nearest DNA methylation probes is about 10,000 base pairs away from the transcription start site. It has been shown that posttranscriptional RNA m^{6}A modification may affect RNA stability and then its level (16, 37). By using miCLIP-seq, we identified a m^{6}A site at exon 6 (1076A) of *WTAPP1* RNA (**Fig. 3A**). Subsequent m^{6}A-specific RNA immunoprecipitation coupled qRT-PCR analysis showed that m^{6}A levels of *WTAPP1* RNA were decreased in cells with downregulation of *METTL3* (**Fig. 3B** and Supplementary Fig. S3B), a well-known m^{6}A writer. In PDAC cells with *METTL3* silenced, overexpression of wild-typed *METTL3* but not its catalytic mutant (38, 39) could restore m^{6}A-*WTAPP1* RNA level (**Fig. 3C**; and Supplementary Fig. S3C). Since recent studies showed that dCas13b-ALKBH5 combined with sgRNAs successfully demethylated specific m^{6}A-RNAs (40, 41), we constructed a similar dm^{6}ACRISPR system (dCas13b-ALKBH5 and gRNAs adjacent to the m^{6}A site of *WTAPP1* RNA) and the results further verified the presence of m^{6}A in *WTAPP1* RNA (**Fig. 3D–E**; Supplementary Fig. S3D).

We next investigated the m^{6}A-*WTAPP1* RNA levels in PDAC of our patient cohorts and found that tumors had significantly higher m^{6}A-*WTAPP1* RNA levels than their adjacent normal tissues (**Fig. 3F**) and advanced PDACs had significantly higher m^{6}A-*WTAPP1* RNA levels than early PDACs (Supplementary Fig. S3E). Furthermore, patients having high m^{6}A-*WTAPP1* RNA level had significantly shorter

Figure 4.

CNBP is a m^{6}A mediator that stabilizes *WTAPP1* RNA. **A,** Scatter plot of proteins in SW1990 and Capan-2 cells that bound to m^{6}A-modified or nonmodified *WTAPP1* probe, both of which were 50-bp oligonucleotides centering on *WTAPP1* RNA m^{6}A site. Unique peptide of ≥ 5 was selected as filter criterium. The diagonal line marks the middle values of *x* and *y* axes. The red point represents CNBP protein. **B,** Western blot analysis showed specific association of m^{6}A-*WTAPP1* RNA with CNBP identified by proteomic screening. **C,** Electrophoretic mobility shift assays of recombinant CNBP with m^{6}A-modified or unmodified *WTAPP1* RNA probes. The reactions were carried out with a constant level of probes and various amount of recombinant CNBP (0–10 μmol/L). **D,** Colocalization of *WTAPP1* RNA and CNBP protein in cells shown by IF. Scale bars, 30 μm. **E** and **F,** Pull-down assays with *in vitro*–transcribed biotin-labeled *WTAPP1* RNA showed binding of *WTAPP1* RNA to whole CNBP or truncated CNBP. Schematic of the domain structures of CNBP protein is shown in **E** and Western blot analysis of FLAG-tagged full-length CNBP or truncated CNBP in 293T cells is shown in **F**. **G,** IGV snapshots showed the CNBP CLIP-seq and miCLIP-seq reads distribution on *WTAPP1* RNA. Purple tracks are unique tag coverage of CNBP CLIP-seq and blue tracks are unique tag coverage of miCLIP-seq, respectively. Filled blue circle denotes miCLIP-called m^{6}A site. **H,** The levels of CNBP bound to *WTAPP1* RNA in PDAC cells with or without *METTL3* knockdown. **I,** The levels of CNBP bound to *WTAPP1* RNA in PDAC cells with *METTL3* knockdown but restored by transfection with WT *METTL3* or its mutant. **J,** Binding levels of CNBP with *WTAPP1* RNA in PDAC cells cotransfected with dCas13b-ALKBH5 and NT-gRNA or sgRNAs. **K** and **L,** Comparison of *WTAPP1* RNA level and its stability in cells with or without CNBP silence. **M,** Immunoprecipitation (IP) assays show CNBP and HuR interaction in PDAC cells. **N,** The levels of HuR bound to *WTAPP1* RNA in cells with or without CNBP silence. **O,** The levels of HuR bound to *WTAPP1* RNA in cells with dm^{6}ACRISPR system. All data are mean ± SEM from three independent experiments. *, $P < 0.05$; **, $P < 0.01$; ***, $P < 0.001$; ns, not significant of Student *t* test.

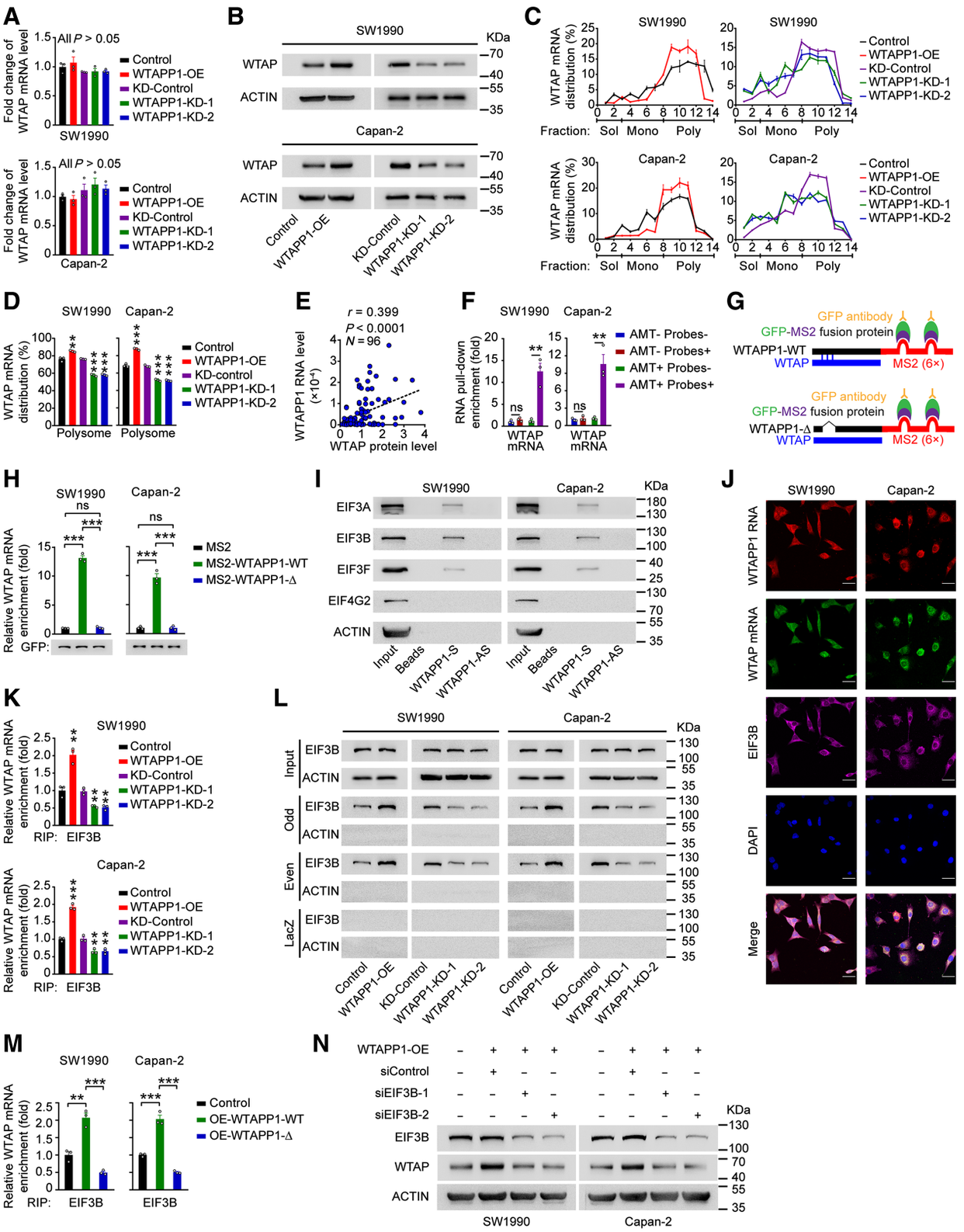
A
Fold change of WTAP mRNA level
All P > 0.05
Control
WTAPP1-OE
KD-Control
WTAPP1-KD-1
WTAPP1-KD-2
SW1990
Capan-2
B
SW1990
KDa
WTAP
ACTIN
Capan-2
Control
WTAPP1-OE
KD-Control
WTAPP1-KD-1
WTAPP1-KD-2
C
WTAP mRNA distribution (%)
SW1990
Capan-2
Fraction: Sol Mono Poly
D
WTAP mRNA distribution (%)
Polysome
E
r = 0.399
P < 0.0001
N = 96
WTAPP1 RNA level (×10⁻⁴)
WTAP protein level
F
RNA pull-down enrichment (fold)
AMT- Probes-
AMT- Probes+
AMT+ Probes-
AMT+ Probes+
WTAP mRNA
G
GFP antibody
GFP-MS2 fusion protein
WTAPP1-WT
WTAP
MS2 (6×)
WTAPP1-Δ
H
Relative WTAP mRNA enrichment (fold)
MS2
MS2-WTAPP1-WT
MS2-WTAPP1-Δ
GFP:
I
EIF3A
EIF3B
EIF3F
EIF4G2
ACTIN
Input
Beads
WTAPP1-S
WTAPP1-AS
J
WTAPP1 RNA
WTAP mRNA
EIF3B
DAPI
Merge
K
RIP: EIF3B
L
Input
Odd
Even
LacZ
M
RIP: EIF3B
OE-WTAPP1-WT
OE-WTAPP1-Δ
N
WTAPP1-OE
siControl
siEIF3B-1
siEIF3B-2
WTAP

survival time than those having low m^{6}A-*WTAPP1* RNA level (Supplementary Fig. S3F). In addition, we grouped PDAC patients into 4 based on the expression patterns of *WTAPP1* m^{6}A and RNA level in PDAC tissues and performed survival analysis and revealed that patients with low *WTAPP1* RNA and m^{6}A levels had better survival compared with those with high *WTAPP1* RNA and/or high m^{6}A levels (Supplementary Fig. S3G). Similar results were obtained when patients were stratified by *METTL3* and *WTAPP1* expression levels (Supplementary Fig. S3H). Furthermore, we also found that *WTAPP1* RNA level was positively correlated with its m^{6}A modification level (**Fig. 3G**).

We then examined the effect of METTL3-mediated m^{6}A formation on the *WTAPP1* levels in cells and found that knockdown of *METTL3* significantly reduced the *WTAPP1* RNA levels (**Fig. 3H**); however, restoration of wild-type (WT) *METTL3* but not its inactive mutant in *METTL3*-knockdown cells could recover the *WTAPP1* RNA levels (**Fig. 3I**). Furthermore, using the dm^{6}ACRISPR system also significantly diminished the *WTAPP1* RNA level in cells (**Fig. 3J**). These results indicate that METTL3-mediated m^{6}A modification may have significant impact on *WTAPP1* RNA stability. Indeed, we explored the stability of *WTAPP1* and found that downregulation of *METTL3* significantly reduced the stability of *WTAPP1*, which could be rescued when WT but not mutant *METTL3* expression was recovered in cells (**Fig. 3K** and **L**). In addition, the dm^{6}A-CRISPR system also decreased the *WTAPP1* stability (**Fig. 3M**). Together, these results suggest that higher *WTAPP1* RNA level in PDAC might be attributed to the enhanced *WTAPP1* RNA stability due to m^{6}A modification.

CNBP recognizes m^{6}A modification of *WTAPP1* and accelerates *WTAPP1* stability

It is well known that deposit of m^{6}A requires a reader to recognize and process the modified RNAs and several proteins such as IGF2BPs and YTHDFs have impact on m^{6}A-modified RNA stability (15, 37). To explore the proteins that may recognize m^{6}A in *WTAPP1* RNA, we performed MS analysis of proteins obtained by RNA pulldown using biotin labeled 50-bp *WTAPP1* or m^{6}A-*WTAPP1* RNA probes and the results showed that in 2 PDAC cell lines, CNBP was the most preferential protein bound to the m^{6}A-*WTAPP1* RNA probe but not *WTAPP1* RNA probe without m^{6}A modification (**Fig. 4A** and Supplementary Data 1), which was verified by Western blot assays (**Fig. 4B**), RNA electrophoretic mobility shift assays (**Fig. 4C**), and immunofluorescence (IF) assays in PDAC cells (**Fig. 4D**).

We constructed various truncated CNBP (**Fig. 4E**) to examine the CNBP domains that bind *WTAPP1* RNA, and found that the amino acid residues 92–134 in CNBP are required for the binding (**Fig. 4F**). CLIP-sequencing of CNBP revealed that CNBP binds to the *WTAPP1* RNA m^{6}A site (**Fig. 4G**). Furthermore, we observed a high binding intensity for CNBP centering at m^{6}A residues and vice versa for the m^{6}A sites. The m^{6}A sites obtained by miCLIP substantially overlapped with CNBP-binding sites obtained by CNBP CLIP-seq (Supplementary Fig. S4A), indicating that CNBP may also recognize m^{6}A sites in RNAs other than m^{6}A-*WTAPP1* RNA.

Next, we examined whether the m^{6}A modification is necessary for the association between CNBP and *WTAPP1* RNA. We found that *METTL3* depletion substantially reduced the interaction of CNBP with *WTAPP1* RNA in cells where CNBP protein-expression level was not altered (**Fig. 4H**; Supplementary Fig. S4B) and restoring WT *METTL3* but not its mutant enhanced the level of CNBP and *WTAPP1* RNA association (**Fig. 4I**). In addition, cells transferred with the dm^{6}A-CRISPR system also showed decreased level of CNBP and *WTAPP1* RNA association (**Fig. 4J**). We also found that CNBP was aberrantly overexpressed in PDAC tumors compared with normal tissues (Supplementary Fig. S4C), which showed the same expression tendency with *WTAPP1* in PDAC tissues. All these results suggest that the association between CNBP and *WTAPP1* RNA is dependent on the m^{6}A modification. Similarly, *CNBP* knockdown substantially reduced the level and stability of *WTAPP1* RNA in cells (**Fig. 4K**, **L** and Supplementary Fig. S4D) and consequently diminished PDAC cell proliferation, migration, and invasion abilities (Supplementary Fig. S4E–S4G), indicating that CNBP is a m^{6}A mediator that plays a role in enhancing the stability and eventually the high level of *WTAPP1* RNA and aggressive phenotype in PDAC cells.

Because m^{6}A readers may enhance the stability of their host RNAs by recruiting cofactors (16), we speculated that the stabilization of *WTAPP1* RNA by CNBP might have the same mechanism. Interestingly, we found that HuR, an RNA stabilizer, was identified by pull-down coupled MS analysis (Supplementary Data S1). Further immunoprecipitation assays confirmed a persisting CNBP and HuR interaction independent on RNA (**Fig. 4M**); RIP assays with HuR antibody revealed that CNBP silence substantially decreased HuR bound to *WTAPP1* RNA (**Fig. 4N**). We also performed RIP assays with HuR antibody in PDAC cells with dm^{6}ACRISPR system and the results showed that decreased *WTAPP1* RNA m^{6}A modification significantly diminished binding of HuR to *WTAPP1* (**Fig. 4O**). These results suggest that CNBP probably recruits RNA stabilizers HuR to promote *WTAPP1* RNA stability.

Figure 5.

WTAPP1 RNA promotes WTAP translation through interacting with *WTAP* mRNA to recruit EIF3 complex. **A,** *WTAP* mRNA levels in PDAC cells with *WTAPP1* expression change. **B,** Western blot analysis of the change of WTAP protein levels in cells with *WTAPP1* overexpression or knockdown. **C** and **D,** Polysome fraction analysis in cells with *WTAPP1* expression change. The level of *WTAP* mRNA in each gradient fraction was measured by qRT-PCR and plotted as a percentage of total *WTAP* mRNA level in that sample (**C**). The translational activity associated with each fraction is indicated as untranslated (Sol, soluble), moderately translated (Mono, monosome), and actively translated (Poly, polysome). Polysome fractions are shown as bar graphs in **D**. **E,** Pearson correlation of the *WTAPP1* RNA and WTAP protein levels in PDAC tissues ($N = 96$). **F,** Enrichment of *WTAP* mRNA in RNA pull-down with *WTAPP1* RNA from PDAC cells. Biotinylated *WTAPP1* RNA probes were incubated with AMT-crosslinked or untreated RNA, the interaction with *WTAPP1* was quantified by qRT-PCR. **G,** Schematic diagram of MS2-RIP assay. Full length (*WTAPP1*-WT; top) or binding sites–deleted *WTAPP1* (*WTAPP1*-Δ, bottom) linked to the MS2 fragments. **H,** MS2-RIP assay shows the levels of *WTAP* mRNA bound to *WTAPP1* RNA in cells with ectopic expression of WT *WTAPP1* (MS2-*WTAPP1*-WT) or *WTAPP1* with binding sites deletion (MS2-*WTAPP1*-Δ). **I,** Western blot showed proteins identified by MS in RNA pull-down assay with biotinylated *WTAPP1* sense or antisense probes. **J,** Colocalization of *WTAPP1* RNA, *WTAP* mRNA, and EIF3B protein revealed by IF assays. Scale bars, 30 μm. **K,** The levels of EIF3B bound to *WTAP* mRNA in cells with *WTAPP1* expression change. **L,** ChIRP assays showed proteins retrieved by *WTAP* mRNA probes labeled with biotin and divided into the odd or even group. After incubation with streptavidin beads, proteins were analyzed by Western blot. LacZ served as the probe negative control while β-ACTIN served as retrieved-protein negative control. **M,** The levels of EIF3B bound to *WTAP* mRNA in cells with ectopic expression of WT *WTAPP1* or binding sites–deleted *WTAPP1*. **N,** Western blot analysis of the WTAP protein level in PDAC cells with *WTAPP1* overexpression and EIF3B silence. All measurement data are from three independent experiments and are represented as mean ± SEM. Student *t* test was used except for the correlation analysis (**E**), which was Pearson test. *, $P < 0.05$; **, $P < 0.01$; ***, $P < 0.001$; ns, not significant.

WTAPP1 promotes WTAP translation by recruiting translation initiation factor EIF3 complex

We next wanted to seek the functional mechanism underlying the oncogenic role of overexpressed *WTAPP1* RNA in PDAC. Since pseudogenes may be involved in regulating their protein-coding counterparts and *WTAPP1* RNA is mainly distributed in cytoplasm of PDAC cells, we speculated that *WTAPP1* RNA might disturb the post-transcriptional regulation or protein translation of its protein-coding counterpart *WTAP* RNA. We found that changing the level of *WTAPP1* RNA did not significantly altered the levels of *WTAP* mRNA; however, it significantly increased WTAP protein level (**Fig. 5A** and **B**), implying that overexpression of *WTAPP1* RNA may promote protein translation of WTAP. We then performed a series of polysome profile analyses and the results showed that *WTAPP1* overexpression increased but knockdown decreased the proportion of *WTAP* mRNA distribution in polysome fraction, without altering the distribution of mRNAs produced by other genes (**Fig. 5C** and **D**; and Supplementary Fig. S5A–S5C), indicating that *WTAPP1* RNA specifically increases the translational efficiency of WTAP. A significant positive correlation between the *WTAPP1* RNA and WTAP protein levels was detected in our 96 clinical PDAC tissue samples (**Fig. 5E**; and Supplementary Fig. S5D).

We then investigated how *WTAPP1* RNA may affect WTAP translation. Based on the public ENCORI data (see URLs) suggesting that *WTAPP1* RNA may interact with *WTAP* mRNA, we assumed that *WTAPP1* RNA might recruit certain proteins to promote WTAP translation via interacting with *WTAP* mRNA. To test this hypothesis, we firstly performed the 4′-AMT assays to verify the interaction of these 2 RNAs. As shown in **Fig. 5F**, *WTAP* mRNA could be retrieved from *WTAPP1* RNA probes in AMT-treated PDAC cells, suggesting that *WTAP* mRNA interacts with *WTAPP1* RNA. Next, we analyzed the binding region of *WTAPP1* using the bibiserv website (see URLs) and the results suggested that a region at exon 1–2 of *WTAPP1* may interact with *WTAP* mRNA (Supplementary Fig. S5E). We then performed MS2-based RIP assays in cells transfected with plasmid containing full length or binding sites delated *WTAPP1* and GFP-MS2 fusion protein (**Fig. 5G**; Supplementary Fig. S5F) and qRT-PCR analysis showed that the *WTAP* mRNA level was greatly elevated in cells with MS2-*WTAPP1*-WT compared with that in cells with empty MS2 or MS2-*WTAPP1*-Δ (**Fig. 5H**), confirming the binding sites of *WTAPP1* is required for its interaction with *WTAP* mRNA.

We then performed RNA pulldown using *WTAPP1* RNA or its antisense probe followed by MS analysis and revealed several translation initiation factors including the components of the EIF3 complex, EIF3B, EIF3A, and EIF3F (Supplementary Data S2), which were confirmed by Western blotting assays (**Fig. 5I**). EIF3 complex consisting of 13 subunits (EIF3A to EIF3M) is essential for initiation of protein synthesis and EIF3B serves as a core scaffolding protein (42–44). Through IF assays, we detected an association of EIF3B with *WTAPP1* and *WTAP* RNAs in the cytoplasm of PDAC cells (**Fig. 5J**). Notably, RIP assays using EIF3B antibody revealed that *WTAPP1* overexpression increased but silence decreased the interaction between EIF3B and *WTAP* mRNA (**Fig. 5K**). Consistent with this result, ChIRP assays also showed that forced change of *WTAPP1* expression specifically increased the interaction of EIF3B with *WTAP* mRNA (**Fig. 5L**; and Supplementary Fig. S5G). Furthermore, we found that overexpression of full-length but not binding site-deleted *WTAPP1* increased EIF3B and *WTAP* mRNA interaction (**Fig. 5M**), suggesting that the interaction of these two RNAs facilitated EIF3B bound to *WTAP* mRNA. Rescue assays verified that the enhanced WTAP translation by *WTAPP1* RNA was EIF3B-dependent since Western blot assays showed that EIF3B knockdown significantly decreased the WTAP protein levels in PDAC cells with *WTAPP1* overexpressed (**Fig. 5N**). Furthermore, we analyzed WTAP protein levels by IHC staining and *WTAPP1* and WTAP RNAs by FISH in clinical tissue samples and found that PDAC with high WTAP protein level also had high *WTAPP1* RNA level, and the 2 types of RNAs were colocalized (Supplementary Fig. S5H).

Collectively, these results demonstrate that overexpressed *WTAPP1* RNA may enhance the recruitment of EIF3B to form more EIF3 complex that promotes WTAP translation.

WTAPP1 is required for WTAP-initiated Wnt signaling activation

WTAP has recently been recognized as an oncoprotein in various types of cancer including PDAC (45–48). By IHC staining of 65 samples (**Fig. 6A**; Supplementary Data 3), we found that WTAP levels were significantly higher in tumors than in paired normal tissues (**Fig. 6B**). Patients with high WTAP level in tumor had significantly shorter survival time than patients with low WTAP level in tumor (**Fig. 6C**). We also grouped PDAC patients into 4 based on the *WTAPP1* RNA and WTAP protein levels and found that patients with low *WTAPP1* RNA and low WTAP protein levels had the best prognosis compared with other groups (Supplementary Fig. S6A). We also performed *in vitro* assays to examine the oncogenic effects of WTAP in PDAC cell lines and revealed that knockdown of WTAP in cells with *WTAPP1* overexpression significantly inhibited cell proliferation, migration, and invasion (**Fig. 6D** and **E**; Supplementary Fig. S6B), suggesting that the effect of *WTAPP1* RNA on malignant phenotypes of PDAC cells is dependent on WTAP.

We next wanted to elucidate the action mechanism in which *WTAPP1* provokes PDAC cell growth and invasiveness by looking at the transcriptomic alterations in PDAC cells with *WTAPP1* knockdown and pathway enrichment of DEGs. Gene ontology analysis suggested that the Wnt signaling pathway was strongly enriched in cells with *WTAPP1* decrease (Supplementary Fig. S6C). Because WTAP has been shown linking to the WT1–TBL1–Wnt signaling axis (48), *WTAPP1* may evoke Wnt signaling. We first tested this notion by analyzing the TCGA data and the results showed that *WTAPP1* is positively correlated with positive regulators (*JAG1, MYC*) and negatively correlated with negative regulators (*HDAC2* and *NKD1*) in the Wnt signaling pathway (Supplementary Fig. S6D). Luciferase reporter assays revealed that increasing *WTAPP1* expression substantially activated the Wnt signaling while suppressing *WTAPP1* expression substantially inhibited this signaling (**Fig. 6F**). Consistent with previous findings that Wnt signaling can target numerous oncogenes and contribute to tumor progression (49–52), we also observed that *WTAPP1* overexpression significantly upregulated the expression of genes downstream the Wnt signaling pathway except for TBL-1, which was downregulated as reported before (48). Opposite results were observed in cells with *WTAPP1* knockdown (**Fig. 6G**). Similarly, WTAP knockdown significantly inhibited the expression of genes downstream the Wnt signaling pathway in cells with *WTAPP1* overexpression (Supplementary Fig. S6E). Furthermore, we found that PDAC cells treated with the dm^{6}ACRISPR system, which depressed *WTAPP1* expression, had substantially lower expression of genes downstream the Wnt signaling pathway compared with control cells (**Fig. 6H**). Overall, these results combined with the results presented above suggest that high level of *WTAPP1* RNA

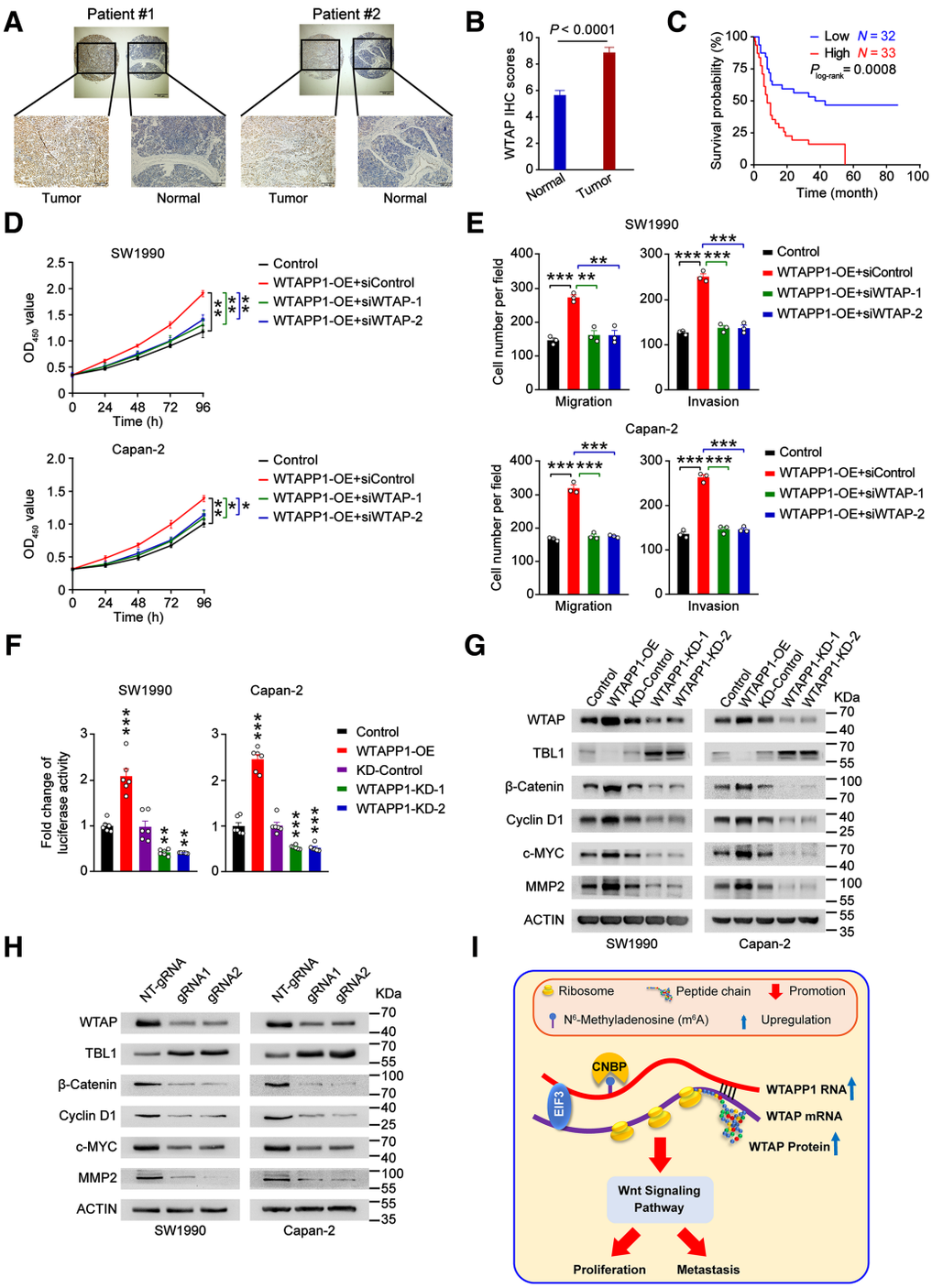

Figure 6.

Wnt signaling is excessively activated in PDAC with *WTAPP1* overexpression. **A,** Representive IHC staining of WTAP proteins in PDAC and paired nontumor tissue samples. Scale bars, 500 μm (top) and 200 μm (bottom). **B,** Quantitative statistics of IHC staining of WTAP in 65 paired PDAC tumor and nontumor tissue samples. *P*, Wilcoxon rank-sum test. **C,** Kaplan–Meier estimates of survival time in PDAC patients by WTAP protein IHC scores in tumor. The adjusted HR for death of high WTAP IHC score was 2.95 (95% CI = 1.57–5.57). **D** and **E,** Effects of WTAP expression knockdown on PDAC cell proliferation (**D**) or migration and invasion (**E**) resulted from *WTAPP1* overexpression. **F,** Reporter gene assays with TCF/LEF1 luciferase and *Renilla* reporter plasmid showed the Wnt signaling activity was significantly altered in PDAC cells when *WTAPP1* expression was changed. **G** and **H,** Western blot analysis demonstrated the expression alteration of signaling molecules downstream of WTAP in PDAC cells when *WTAPP1* expression was changed (**G**) or transfected with dm^{6}ACRISPR system (**H**). Data in **D–F** are mean ± SEM from three independent experiments. **, $P < 0.01$; ***, $P < 0.001$ of Student *t* test. **I,** A proposed action model for excessive *WTAPP1* RNA level caused by the RNA m^{6}A modification in the progression of PDAC.

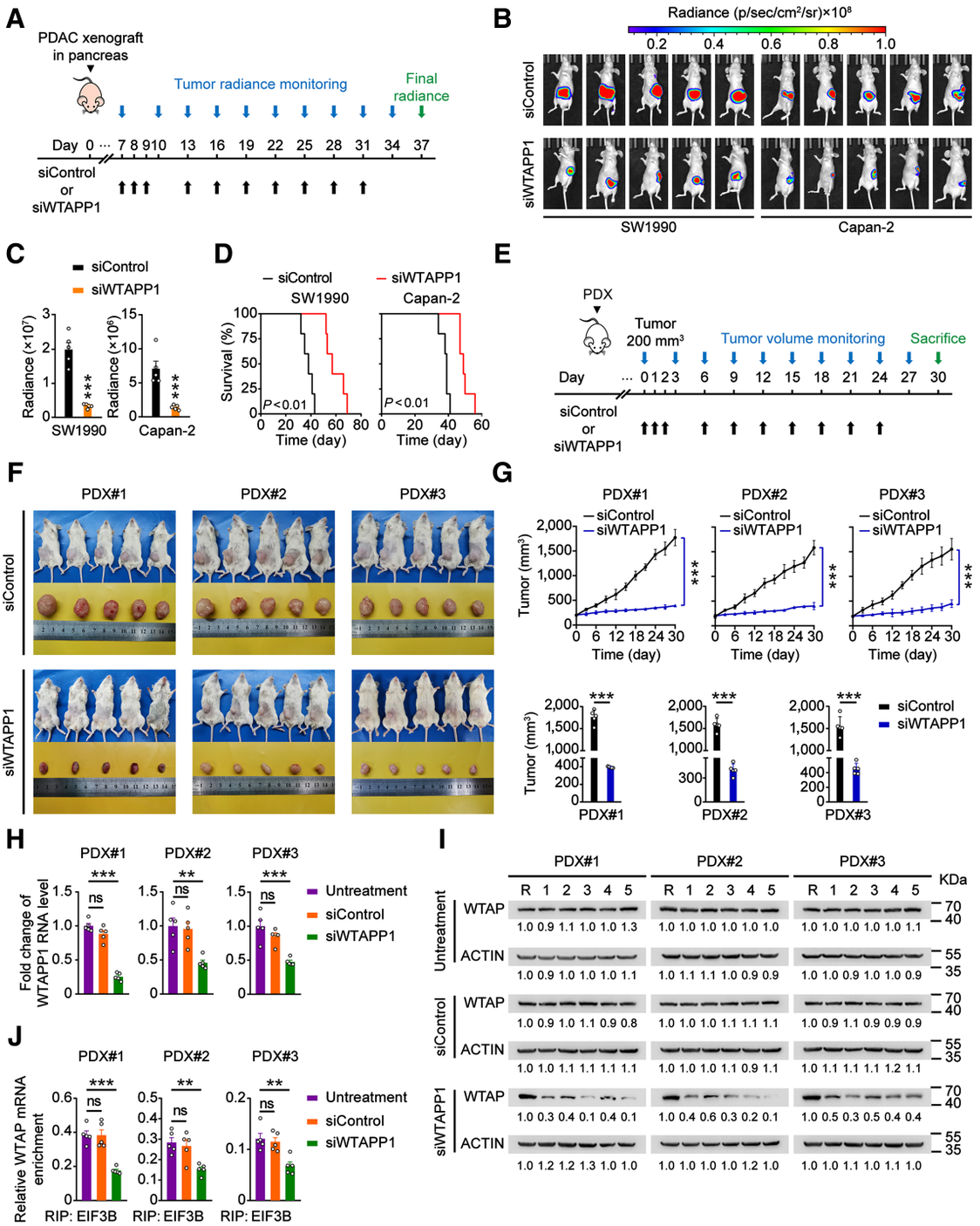

Figure 7.

WTAPP1 RNA is a therapeutic target in mouse PDAC xenografts. **A,** Timeline schematic for treatment of mice carrying PDAC xenograft in the pancreas with siWTAPP1. Colored arrows indicate the times when different events occurred. **B** and **C,** Administration of siWTAPP1 via tail vein significantly suppressed tumor growth and metastasis. Shown are the radiant images of xenograft in mice ($N = 5$; **B**) and tumor growth rate expressed as radiance intensity (**C**). **D,** Survival times of mice treated with or without siWTAPP1. **E,** Timeline schematic for treatment of mice with PDX. Colored arrows indicate the times when different events occurred. **F,** Shown are the images of PDXs from three patients in 5 mice. **G,** Tumor growth curves (top) and tumor volumes in the end of experiment (bottom), with administration of siWTAPP1 via tail vein. **H–J,** Effects of siWTAPP1 treatment on *WTAPP1* RNA level determined by qRT-PCR (**H**), WTAP protein level analyzed by Western blotting (**I**), and the ability of EIF3B bound to *WTAP* mRNA detected by EIF3B RIP-qPCR (**J**). R in **I** stands for the same positive reference sample for loading adjustment on each gel. Each protein band was semiquantified by gray density and the value for each band is relative to density of corresponding band of R. Data in **G** represent mean ± SD and other measurements are mean ± SEM. **, $P < 0.01$; ***, $P < 0.001$; ns, not significant of Student *t* test.

resulted from the excessive m^{6}A modification may activate the Wnt signaling in PDAC pathogenic processes (**Fig. 6I**).

WTAPP1 is a therapeutic target in mouse xenograft tumors

Because *WTAPP1* shows a strong oncogenic effect in PDAC cells, we established xenografts derived from *WTAPP1*-upregulated PDAC luciferase-expressing cells in mice and treated the animals with *in vivo*–optimized siWTAPP1 (**Fig. 7A**). We found that treatment of siWTAPP1 (75 mg/kg, i.v.) significantly reduced tumor burden and prolonged survival time of mice compared with siControl (**Fig. 7B–D**). We also established PDXs in mice and performed similar siWTAPP1 treatment (**Fig. 7E**). The results showed that administration of siWTAPP1 significantly reduced PDX growth rates compared with administration of siControl. The siWTAPP1 reagent showed no apparent toxicity to mice since the animals had no significant bodyweight reduction (**Fig. 7F** and **G**; Supplementary Fig. S6F). The qRT-PCR and Western blot analyses confirmed that treatment of siWTAPP1 effectively inhibited *WTAPP1* RNA and WTAP protein expressions and reduced the binding ability of EIF3B with *WTAP* mRNA in PDXs (**Fig. 7H–J**). These results strong suggest that *WTAPP1* may be a therapeutic target for PDAC treatment.

Discussion

In this study, we have identified a panel of aberrantly expressed pseudogenes in PDAC and among them, *WTAPP1* has the strongest effect on PDAC-malignant phenotypes as demonstrated by our function screening. We found that *WTAPP1* RNA level is significantly higher in PDAC and the increased level is associated with shorter survival time in patients. *WTAPP1* RNA is stabilized by m^{6}A modification and the excessive *WTAPP1* RNA level may promote the EIF3 complex formation to enhance oncoprotein WTAP translation, which excessively activates Wnt signaling that plays a role in PDAC. Several novel findings have been achieved in this study. First, we have found for the first time that pseudogene *WTAPP1* RNA level is elevated by aberrant m^{6}A modification and plays an oncogenic role in human PDAC. Second, we have identified CNBP as the potential m^{6}A reader that stabilizes WTAPP1 RNA. Third, we have revealed that *WTAPP1* RNA can interact with EIF3B to promote the formation of translation initiation complex that enhance WTAP translation, which links to the activation of Wnt signaling in PDAC progression.

Accumulating evidence has suggested that pseudogene produced RNAs may play diverse roles in physiological and pathological processes, especially in cancer (5, 6). Up to date, there have been two studies reporting *WTAPP1* produced RNA that plays an oncogenic role in laryngeal and lung cancer (53, 54). Here, we report that *WTAPP1* RNA is significantly upregulated in PDAC, which is associated with poor prognosis of PDAC patients. Therefore, our findings in the current study provide additional evidence supporting *WTAPP1* as an oncogenic pseudogene in cancer. More importantly, we have performed comprehensive functional analyses to discover the underlying molecular mechanism for the action of this oncogenic pseudogene in PDAC. The results have extended our knowledge about the role of this class of genomic makeup. Furthermore, we have demonstrated that the oncogenic role of *WTAPP1* RNA in PDAC can be targeted and suppressed by siWTAPP1. This information might also be interesting for the drug and treatment option development of PDAC.

We have revealed that the elevated level of *WTAPP1* RNA in PDAC is resulted from aberrant m^{6}A modification, which significantly increases the RNA stability. Several previous studies have also suggested this mechanism for some oncogenic RNA (10, 15, 16, 37); however, little has been known about the m^{6}A modification in PDAC (12, 13). In view of our findings that *WTAPP1* RNA is aberrantly m^{6}A-modified, it would be interesting and important to fully characterize the m^{6}A modification at whole-transcriptome level in PDAC and to further discover the underlying mechanism for the formation and the consequences of this epigenetic modification. In addition to this, there might be other mechanisms such as microRNA interaction attributable to the aberrant *WTAPP1* level in PDAC, which would be interesting to investigate.

The biological importance of m^{6}A modification relies on m^{6}A-binding proteins (readers) and previous studies have reported several RNA-binding proteins as m^{6}A readers, such as YTH domain-containing proteins and IGF2BP proteins (16, 37). In the present study, we have shown that CNBP preferentially interacts with and stabilizes m^{6}A-modified *WTAPP1* RNA. CNBP is an RNA-binding protein and transcription factor that contains seven highly conserved zinc finger domains involving in RNA transcription, stabilization, and translation (55, 56). It has been shown that under the guidance of lncRNA LAST, CNBP binds to and stabilizes CCND1 mRNA (55). In this study, we have found by several experimental setting that CNBP is likely an m^{6}A reader that recognizes the m^{6}A modification in *WTAPP1* RNA. By analyzing the published data (57), we have also revealed that CNBP preferentially binds the GGm^{6}ACU site in the probes in both HeLa cells and mouse 3T3 cells. The consistency of our results with others indicates that CNBP may be a common reader recognizing the m^{6}A sites in various RNAs, which is warranted to further investigation.

ncRNAs transcribed by pseudogenes play diverse roles in posttranscriptional regulation of many protein-coding genes as antisense RNAs, endogenous siRNAs, and competing endogenous RNAs (5, 6, 8). For example, it has been shown that neural nitric oxide synthase (nNOS) mRNA can directly bind RNA produced by its pseudogene to form double-strand RNA–RNA duplex and consequently diminish nNOS mRNA translation (58). In this study, we have demonstrated that *WTAPP1* RNA has ability to promote WTAP translation, providing a new acting model for pseudogenes.

WTAP has increasingly attracted the research attention because of its oncogenic role in various types of malignancies including PDAC (45–48). In addition to its function as a RNA methyltransferase, WTAP also plays a carcinogenic role through activating signaling pathways. For instance, it has been shown that WTAP may activate the Wnt signaling pathway by inhibiting *TBL1* transcription and reducing β-catenin degradation in colorectal cancer (48). Because excessive *WTAPP1* RNA promotes WTAP protein translation, one may expect that Wnt signaling would be aberrantly enhanced in PDAC, which has previously been observed in PDAC (49, 50). We have really demonstrated that increased *WTAPP1* RNA significantly evokes the Wnt signaling via increasing WTAP and suppressing TBL-1, which is probably a molecular mechanism for PDAC development and progression. Because the Wnt signaling pathway plays an important role in many other cancers, it would be interesting to explore whether *WTAPP1* has the same function in other types of cancer.

Because *WTAPP1* RNA shows oncogenic effect and its levels increase in a disease stage–dependent manner, we assumed that it may be a valuable therapeutic target for PDAC. Indeed, in xenograft models, we are able to show that administration of siWTAPP1 significantly reduced the growth rate and distant metastasis of PDAC in mice. The efficacy of siWTAPP1 administration in xenografts may suggest a potential option for the development of PDAC treatment although further investigations are needed such as

systematical evaluation of the potential toxicity caused by *WTAPP1* inhibition.

In conclusion, we have identified *WTAPP1* as an oncogenic pseudogene in PDAC acting via promoting the translation of WTAP protein, a molecule that activates Wnt signaling. *WTAPP1* RNA can be stabilized by aberrant m^6A modification mediated by CNBP. PDAC cell growth and invasiveness *in vitro* and *in vivo* can be suppressed by siWTAPP1, highlighting that *WTAPP1* may serve as a potential novel therapeutic target for PDAC.

Authors' Disclosures

X. Huang reports grants from Natural Science Foundation of China during the conduct of the study. D. Lin reports grants from Natural Science Foundation of China during the conduct of the study. J. Zheng reports grants from Natural Science Foundation of China during the conduct of the study. No disclosures were reported by the other authors.

Authors' Contributions

J. Deng: Data curation, formal analysis, validation, visualization, methodology, writing–original draft, writing–review and editing. **J. Zhang:** Formal analysis, validation, visualization, methodology. **Y. Ye:** Data curation, software, formal analysis, visualization, methodology. **K. Liu:** Methodology. **L. Zeng:** Methodology. **J. Huang:** Data curation, formal analysis. **L. Pan:** Methodology. **M. Li:** Methodology. **R. Bai:** Methodology. **L. Zhuang:** Methodology. **X. Huang:** Funding acquisition, methodology. **G. Wu:** Methodology. **L. Wei:** Methodology. **Y. Zheng:** Methodology. **J. Su:** Methodology. **S. Zhang:** Methodology. **R. Chen:** Conceptualization, supervision, project administration. **D. Lin:** Conceptualization, supervision, funding acquisition, writing–original draft, project administration, writing–review and editing. **J. Zheng:** Conceptualization, supervision, funding acquisition, writing–original draft, project administration, writing–review and editing.

Acknowledgments

This study was supported by the Natural Science Foundation of China (81772586, 82072617 to J. Zheng; 81802407 to X. Huang; and 91753142 to D. Lin), Program for Guangdong Introducing Innovative and Entrepreneurial Teams (2017ZT07S096 to D. Lin), National Young Top-notch Talent Support Program (to J. Zheng), Natural Science Foundation of Guangdong Province (2018A030313327 to X. Huang), and Sun Yat-sen University Intramural Funds (to D. Lin and to J. Zheng).

Note

Supplementary data for this article are available at Cancer Research Online (http://cancerres.aacrjournals.org/).

Received February 15, 2021; revised June 26, 2021; accepted August 3, 2021; published first August 6, 2021.

References

1. Siegel RL, Miller KD, Jemal A. Cancer statistics, 2020. CA Cancer J Clin 2020;70:7–30.
2. Grossberg AJ, Chu LC, Deig CR, Fishman EK, Hwang WL, Maitra A, et al. Multidisciplinary standards of care and recent progress in pancreatic ductal adenocarcinoma. CA Cancer J Clin 2020;70:375–403.
3. Mizrahi JD, Surana R, Valle JW, Shroff RT. Pancreatic cancer. Lancet 2020;395:2008–20.
4. Kalyana-Sundaram S, Kumar-Sinha C, Shankar S, Robinson DR, Wu YM, Cao X, et al. Expressed pseudogenes in the transcriptional landscape of human cancers. Cell 2012;149:1622–34.
5. Lu X, Gao A, Ji L, Xu J. Pseudogene in cancer: real functions and promising signature. J Med Genet 2015;52:17–24.
6. Karreth FA, Reschke M, Ruocco A, Ng C, Chapuy B, Leopold V, et al. The BRAF pseudogene functions as a competitive endogenous RNA and induces lymphoma in vivo. Cell 2015;161:319–32.
7. Cheetham SW, Faulkner GJ, Dinger ME. Overcoming challenges and dogmas to understand the functions of pseudogenes. Nat Rev Genet 2020;21:191–201.
8. Poliseno L, Salmena L, Zhang J, Carver B, Haveman WJ, Pandolfi PP. A coding-independent function of gene and pseudogene mRNAs regulates tumour biology. Nature 2010;465:1033–8.
9. Huang H, Weng H, Chen J. m(6)A Modification in coding and non-coding RNAs: Roles and therapeutic implications in cancer. Cancer Cell 2020;37:270–88.
10. Deng X, Su R, Weng H, Huang H, Li Z, Chen J. RNA N (6)-methyladenosine modification in cancers: current status and perspectives. Cell Res 2018;28:507–17.
11. Zhang S, Zhao BS, Zhou A, Lin K, Zheng S, Lu Z, et al. m(6)A Demethylase ALKBH5 maintains tumorigenicity of glioblastoma stem-like cells by sustaining FOXM1 expression and cell proliferation program. Cancer Cell 2017;31:591–606.
12. He Y, Hu H, Wang Y, Yuan H, Lu Z, Wu P, et al. ALKBH5 inhibits pancreatic cancer motility by decreasing long non-coding RNA KCNK15-AS1 methylation. Cell Physiol Biochem 2018;48:838–46.
13. Zhang J, Bai R, Li M, Ye H, Wu C, Wang C, et al. Excessive miR-25–3p maturation via N (6)-methyladenosine stimulated by cigarette smoke promotes pancreatic cancer progression. Nat Commun 2019;10:1858.
14. Zaccara S, Ries RJ, Jaffrey SR. Reading, writing and erasing mRNA methylation. Nat Rev Mol Cell Biol 2019;20:608–24.
15. Yang Y, Hsu PJ, Chen YS, Yang YG. Dynamic transcriptomic m(6)A decoration: writers, erasers, readers and functions in RNA metabolism. Cell Res 2018;28:616–24.
16. Huang H, Weng H, Sun W, Qin X, Shi H, Wu H, et al. Recognition of RNA N (6)-methyladenosine by IGF2BP proteins enhances mRNA stability and translation. Nat Cell Biol 2018;20:285–95.
17. Pan T. N6-methyl-adenosine modification in messenger and long non-coding RNA. Trends Biochem Sci 2013;38:204–9.
18. Yang D, Qiao J, Wang G, Lan Y, Li G, Guo X, et al. N6-Methyladenosine modification of lincRNA 1281 is critically required for mESC differentiation potential. Nucleic Acids Res 2018;46:3906–20.
19. Patil DP, Chen CK, Pickering BF, Chow A, Jackson C, Guttman M, et al. m(6)A RNA methylation promotes XIST-mediated transcriptional repression. Nature 2016;537:369–73.
20. Liu N, Zhou KI, Parisien M, Dai Q, Diatchenko L, Pan T. N6-methyladenosine alters RNA structure to regulate binding of a low-complexity protein. Nucleic Acids Res 2017;45:6051–63.
21. Zhou KI, Parisien M, Dai Q, Liu N, Diatchenko L, Sachleben JR, et al. N(6)-methyladenosine modification in a long noncoding RNA hairpin predisposes its conformation to protein binding. J Mol Biol 2016;428:822–33.
22. Martin M. Cutadapt removes adapter sequences from high-throughput sequencing reads. EMBnet J 2011;17:10–2.
23. Li B, Dewey CN. RSEM: accurate transcript quantification from RNA-Seq data with or without a reference genome. BMC Bioinformatics 2011;12:323.
24. Frankish A, Diekhans M, Ferreira AM, Johnson R, Jungreis I, Loveland J, et al. GENCODE reference annotation for the human and mouse genomes. Nucleic Acids Res 2019;47:D766–D73.
25. Love MI, Huber W, Anders S. Moderated estimation of fold change and dispersion for RNA-seq data with DESeq2. Genome Biol 2014;15:550.
26. Mueller MT, Hermann PC, Witthauer J, Rubio-Viqueira B, Leicht SF, Huber S, et al. Combined targeted treatment to eliminate tumorigenic cancer stem cells in human pancreatic cancer. Gastroenterology 2009;137:1102–13.
27. Rubio-Viqueira B, Jimeno A, Cusatis G, Zhang X, Iacobuzio-Donahue C, Karikari C, et al. An in vivo platform for translational drug development in pancreatic cancer. Clin Cancer Res 2006;12:4652–61.
28. Tadros S, Shukla SK, King RJ, Gunda V, Vernucci E, Abrego J, et al. De novo lipid synthesis facilitates gemcitabine resistance through endoplasmic reticulum stress in pancreatic cancer. Cancer Res 2017;77:5503–17.
29. Moore MJ, Zhang C, Gantman EC, Mele A, Darnell JC, Darnell RB. Mapping argonaute and conventional RNA-binding protein interactions with RNA at single-nucleotide resolution using HITS-CLIP and CIMS analysis. Nat Protoc 2014;9:263–93.
30. Webb S, Hector RD, Kudla G, Granneman S. PAR-CLIP data indicate that Nrd1-Nab3-dependent transcription termination regulates expression of hundreds of protein coding genes in yeast. Genome Biol 2014;15:R8.

31. Li H, Durbin R. Fast and accurate short read alignment with Burrows-Wheeler transform. Bioinformatics 2009;25:1754–60.
32. Shah A, Qian Y, Weyn-Vanhentenryck SM, Zhang C. CLIP Tool Kit (CTK): a flexible and robust pipeline to analyze CLIP sequencing data. Bioinformatics 2017;33:566–7.
33. Linder B, Grozhik AV, Olarerin-George AO, Meydan C, Mason CE, Jaffrey SR. Single-nucleotide-resolution mapping of m6A and m6Am throughout the transcriptome. Nat Methods 2015;12:767–72.
34. Robinson JT, Thorvaldsdottir H, Winckler W, Guttman M, Lander ES, Getz G, et al. Integrative genomics viewer. Nat Biotechnol 2011;29:24–6.
35. Yu G, Wang LG, Han Y, He QY. clusterProfiler: an R package for comparing biological themes among gene clusters. OMICS 2012;16:284–7.
36. Wang Y, He L, Du Y, Zhu P, Huang G, Luo J, et al. The long noncoding RNA lncTCF7 promotes self-renewal of human liver cancer stem cells through activation of Wnt signaling. Cell Stem Cell 2015;16:413–25.
37. Wang X, Lu Z, Gomez A, Hon GC, Yue Y, Han D, et al. N6-methyladenosine-dependent regulation of messenger RNA stability. Nature 2014;505:117–20.
38. Lin S, Choe J, Du P, Triboulet R, Gregory RI. The m(6)A methyltransferase METTL3 promotes translation in human cancer cells. Mol Cell 2016;62:335–45.
39. Wang Q, Chen C, Ding Q, Zhao Y, Wang Z, Chen J, et al. METTL3-mediated m(6)A modification of HDGF mRNA promotes gastric cancer progression and has prognostic significance. Gut 2020;69:1193–205.
40. Li Z, Peng Y, Li J, Chen Z, Chen F, Tu J, et al. N (6)-methyladenosine regulates glycolysis of cancer cells through PDK4. Nat Commun 2020;11:2578.
41. Li J, Chen Z, Chen F, Xie G, Ling Y, Peng Y, et al. Targeted mRNA demethylation using an engineered dCas13b-ALKBH5 fusion protein. Nucleic Acids Res 2020;48:5684–94.
42. Marintchev A, Wagner G. Translation initiation: structures, mechanisms and evolution. Q Rev Biophys 2004;37:197–284.
43. Hinnebusch AG. eIF3: a versatile scaffold for translation initiation complexes. Trends Biochem Sci 2006;31:553–62.
44. ElAntak L, Tzakos AG, Locker N, Lukavsky PJ. Structure of eIF3b RNA recognition motif and its interaction with eIF3j: structural insights into the recruitment of eIF3b to the 40 S ribosomal subunit. J Biol Chem 2007;282:8165–74.
45. Li BQ, Huang S, Shao QQ, Sun J, Zhou L, You L, et al. WT1-associated protein is a novel prognostic factor in pancreatic ductal adenocarcinoma. Oncol Lett 2017;13:2531–8.
46. Li BQ, Liang ZY, Seery S, Liu QF, You L, Zhang TP, et al. WT1 associated protein promotes metastasis and chemo-resistance to gemcitabine by stabilizing Fak mRNA in pancreatic cancer. Cancer Lett 2019;451:48–57.
47. Chen Y, Peng C, Chen J, Chen D, Yang B, He B, et al. WTAP facilitates progression of hepatocellular carcinoma via m6A-HuR-dependent epigenetic silencing of ETS1. Mol Cancer 2019;18:127.
48. Zhang J, Tsoi H, Li X, Wang H, Gao J, Wang K, et al. Carbonic anhydrase IV inhibits colon cancer development by inhibiting the Wnt signalling pathway through targeting the WTAP-WT1-TBL1 axis. Gut 2016;65:1482–93.
49. Li L, Li Z, Kong X, Xie D, Jia Z, Jiang W, et al. Down-regulation of microRNA-494 via loss of SMAD4 increases FOXM1 and beta-catenin signaling in pancreatic ductal adenocarcinoma cells. Gastroenterology 2014;147:485–97.
50. Morris JP 4th, Wang SC, Hebrok M. KRAS, Hedgehog, Wnt and the twisted developmental biology of pancreatic ductal adenocarcinoma. Nat Rev Cancer 2010;10:683–95.
51. Clevers H, Nusse R. Wnt/beta-catenin signaling and disease. Cell 2012;149:1192–205.
52. Peng K, Kou L, Yu L, Bai C, Li M, Mo P, et al. Histone demethylase JMJD2D Interacts With beta-catenin to induce transcription and activate colorectal cancer cell proliferation and tumor growth in mice. Gastroenterology 2019;156:1112–26.
53. Shi XY, Lin JJ, Ge XJ, Shi Y. LncRNA WTAPP1 promotes proliferation of laryngeal carcinoma cells through regulating microRNA-592. Eur Rev Med Pharmacol Sci 2020;24:9532–40.
54. Zhang L, Jin C, Yang G, Wang B, Hua P, Zhang Y. LncRNA WTAPP1 promotes cancer cell invasion and migration in NSCLC by downregulating lncRNA HAND2-AS1. BMC Pulm Med 2020;20:153.
55. Cao L, Zhang P, Li J, Wu M. LAST, a c-Myc-inducible long noncoding RNA, cooperates with CNBP to promote CCND1 mRNA stability in human cells. Elife 2017;6:e30433.
56. Lee E, Lee TA, Kim JH, Park A, Ra EA, Kang S, et al. CNBP acts as a key transcriptional regulator of sustained expression of interleukin-6. Nucleic Acids Res 2017;45:3280–96.
57. Edupuganti RR, Geiger S, Lindeboom RGH, Shi H, Hsu PJ, Lu Z, et al. N (6)-methyladenosine (m(6)A) recruits and repels proteins to regulate mRNA homeostasis. Nat Struct Mol Biol 2017;24:870–8.
58. Korneev SA, Park JH, O'Shea M. Neuronal expression of neural nitric oxide synthase (nNOS) protein is suppressed by an antisense RNA transcribed from an NOS pseudogene. J Neurosci 1999;19:7711–20.